Journal of Materials Chemistry A

Accepted Manuscript

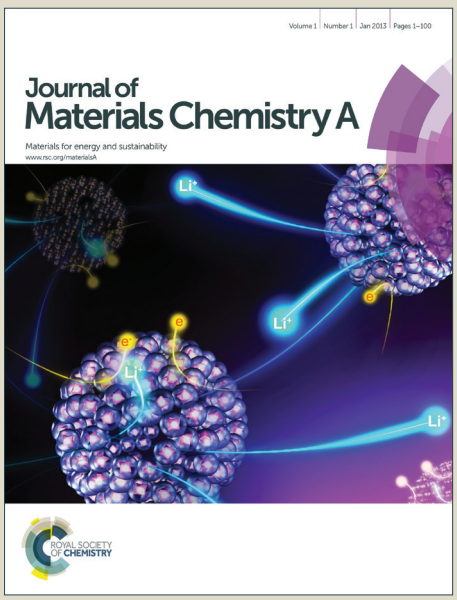

ROYAL SOCIETY OF CHEMISTRY

www.rsc.org/materialsA

Cite this: DOI: 10.1039/c0xx00000x

www.rsc.org/xxxxxx

ARTICLE TYPE

Highly conductive carbon-CoO hybrid nanostructured arrays with enhanced electrochemical performance for asymmetric supercapacitors

Hai Wang, Chen Qing, Junling Guo, A.A. Aref , Daming Sun, Bixiao Wang and Yiwen Tang*

Received (in XXX, XXX) Xth XXXXXXXXX 20XX, Accepted Xth XXXXXXXXX 20XX

DOI: 10.1039/b000000x

In this work, we report the synthesis of hybrid nanowire arrays by growing highly conductive carbon onto rough CoO nanowire arrays on 3D nickel foam. The CoO@C nanostructured arrays (CCNAs) are obtained via a hydrothermal method, followed by controlling the annealing and carbon deposition process at a relatively low temperature in chemical vapor deposition (CVD) stage. The carbon shell, apart from partial amorphous carbon, the crystalline conductive carbon shell was observed. With deposited carbon, the electrical conductivity and capacitance behaviors are dramatically promoted. The growth mechanism is proposed by TEM and XPS analysis, which firstly indicates that CoO could catalyze the decomposition of C_2H_2 at a low temperature of 427 ℃ in a reduction and catalytic process. The obtained CCNAs with a more hydrophilic surface and low resistance are tested as the working electrodes of supercapacitors, which lead to an ultrahigh specific capacitance of 3282.2 F g^{-1} approaching to the theoretical value. Good rate capability and 96.9% capacitance retention after 10000 cycles suggest that such hybrid electrode possesses a great potential application. After assembling it as positive electrode and activated carbon as the negative electrode, the aqueous asymmetric supercapacitor demonstrates energy density up to (~58.9 Wh kg^{-1}) which is the highest received among the Co-based supercapacitors.

1 Introduction

Continuous increasing energy demand has facilitated recent research on energy-storage devices. Supercapacitors, with its longer lifespan, better safety and faster charge-discharge capability, are considering as the most promising power devices.[1] Carbon materials, conducting polymers and metal oxides materials are conventional employed ones based on different energy storage principles respectively. Carbon materials, with high conductivity, store charge by reversible adsorption of ions at the interface of electrode and the electrolyte, which makes high power supply but low energy density. Oppositely, through redox reaction in faradaic process, metal oxides-based materials get much higher specific capacitance, however, high resistance makes it hard to completely represent their intrinsic ability.[2]

Among kinds of metal oxides, CoO, Co_3O_4, NiO, RuO_2, MnO_2,[3-7] have been widely investigated. Cobalt oxides, because of its high theoretical capacitances larger than 4000 F g^{-1} [8] and comparatively low cost, receive intense attentions. In order to enhance their capacitance ability, efforts have been made to increase the surface area and reduce intrinsic resistance for limited ion diffusion in bulk materials and poor electron transfer as semiconducting compounds. Cobalt oxides nanoparticles and arrays have been synthesized and obtain relatively high electrochemical property. Besides merely increasing the surface area, composites to augment the electrical conductivity through combination with reduced graphene oxide,[9] carbon nanotubes,[10] carbon nanomembrane,[11] polypyrrole,[8] carbon microspheres,[12] also further give a performance improvement. However, such composite patterns give no really a boost to the capacitance improvement, for the composite behaviors of these materials are not totally contacted with the active material or merely giving a limited promotion in electrical conductivity.

Carbon nanotubes, graphene, graphite, activated carbon, of which raw material available extensively in the nature, are hot research topics in electronic or electrochemical applications.[13-15] As is known to all, either graphite carbon or graphene carbon (~10^6 S cm^{-1})[16] leads to much higher electrical conductivity than CoO (~10^{-2} S cm^{-1}).[17] Considering the above aspects, CoO@C nanostructured arrays (CCNAs) are designed as conductive carbon integrated high capacity rough cobalt monoxides nanowires which directly grow on 3D nickel foam current collector. Such process is synthesized in a low temperature in-situ chemical vapor deposition (CVD) method. The designed CCNAs possess following advantages: (i) CoO not only is a capacitor material, but also firstly convinced as a catalyst to catalyze the decomposition of acetylene (C_2H_2) in a reduction and catalytic process during the CVD process. (ii) In current works, for thin carbon coatings as core/shell structures, the most obtained carbon shell synthesized in various methods is amorphous. Such as CoO@C[18], ZnO@C[19] (CVD method); MnO_2@C[20a] (hydrothermal and annealing method), Co_3O_4@C[20b] (current magnetron sputtering method). However, in this work, apart from partial amorphous carbon, the crystalline conductive carbon shell

is observed. (iii) Both of the components are electrical active and complementary. Along with the improving of electrical conductivity, the electrochemical reaction ions are easier to be absorbed on the surface of active material, leading to enhanced redox reaction and the capacitance is further promoted. As a consequence, the optimized CCNAs exhibit a highest specific capacitance of 3277.4 F g^{-1} (6.76 F cm^{-2}) at current density of 1 mA cm^{-2} which is the highest specific capacitance to date to our best knowledge. Even at a high current density of 50 mA cm^{-2}, the CCNAs remain 1481.6 F g^{-1} and show little capacitance loss after 10000 cycles. To further confirm the practical capacitance behavior, an asymmetric supercapacitor was assembled using the optimized CCNAs as positive electrode and activated carbon (AC) film on nickel foam as negative electrode. It delivers a maximum energy density and power density of 58.89 Wh kg^{-1} (5 mA) and 3186.5 W kg^{-1} (100 mA). Such outstanding behaviors imply the CCNAs are really promising practical energy-storage materials.

2 Experimental

2.1 Material synthesis

The brief fabrication procedure of hybrid CCNAs is illustrated in Fig. 1.

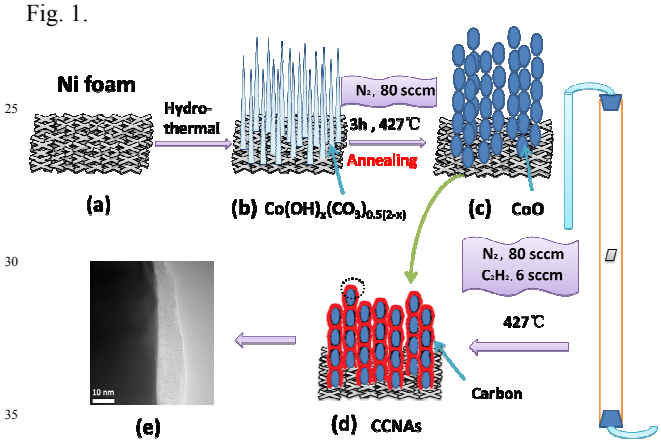

Fig. 1 The fabrication procedure of hybrid CCNAs: (a) Nickel foam substrate; (b) The precursor $Co(OH)_x(CO_3)_{0.5(2-x)}$ array; (c) CoO nanowires array; (d) CCNAs; (e) TEM image of the edge of CCNAs-150s.

Synthesis of precursor $Co(OH)_x(CO_3)_{0.5(2-x)}$ nanowire arrays on nickel foam. The precursor $Co(OH)_x(CO_3)_{0.5(2-x)}$ were firstly synthesized using a facile hydrothermal method according to previous article.[9] The fabrication procedure of hybrid CCNAs is illustrated in Fig. 1. In brief, 0.727 g cobalt nitrate hexahydrate and 0.7 g urea were dissolved in 50 mL deionized water and stirring for 10 minutes at room temperature. Then the homogeneous solution was transferred into Teflon-lined stainless steel autoclave. A piece of 20×50×1.1 mm^3 clean nickel foam used as current collector and substrate material was immersed into the reaction solution. The autoclave was sealed and maintained in an electric oven at 95 ℃ for 8 h. After the reaction, nickel foam with array was rinsed with deionized water for several times and dried at 60 ℃ for 5 h.

Synthesis of CoO nanowire arrays on nickel foam. To obtain pure CoO nanowire array, the precursor was transferred into a quartz tube furnace. In an atmosphere of N_2 at the flow rate of 80 sccm, the sample was heated to 427 ℃ (700 K) in an hour and held for 3 h to completely convert into CoO nanowire arrays. Finally, the sample was cooled down to room temperature naturally and taken out. The obtained product (pure CoO nanowire arrays) is denoted as CCNAs-0s.

Synthesis of CCNAs on nickel foam. In order to get CCNAs, the precursor was also transferred into a quartz tube furnace. In the same atmosphere of N_2 at the flow rate of 80 sccm, the sample was heated to 427 ℃ (700 K) in an hour and held for 3 h for its transformation to CoO. Subsequently, C_2H_2 was introduced immediately at the flow rate of 6 sccm for 150 s with the N_2 unchanged all the time. Then with atmosphere of N_2, the sample was cooled down to room temperature naturally. The obtained product is denoted as CCNAs-150s. Similarly, CCNA-120s, CCNA-180s and CCNA-240s were obtained by introducing C_2H_2 for 120 s, 180 s and 240 s, respectively.

For purpose of assembling an asymmetric supercapacitor, an active carbon electrode was prepared as negative electrode. This electrode was prepared by mixing 90% activated carbon and 10% PTFE, then casting onto a 1×1 cm^2 nickel foam with different total mass. After pressing the negative electrode at 6 M Pa, CCNAs (positive electrode) were connected to form a full cell in the electrolyte of 6 M KOH.

2.2 Materials characterizations

The products were characterized using X-ray diffraction (XRD, PANalytical Empyrean, Cu Kα radiation; λ=1.5418 Å), field-emission scanning electron microscopy (FESEM, JEOL JSM-6700F, 10 kV), transmission electron microscopy (TEM, Titan G2 60-300), X-ray energy-dispersive spectroscope (EDS) attached to a TEM, Raman spectroscopy (LabRAM HR evolution with laser excitation at 532 nm). X-ray photoelectron spectroscopy (XPS) was carried out using VG Multilab 2000 by setting the peak corresponding to carbon to 284.6 eV. The mass of electrode materials was measured on an AX/MX/UMX Balance (METTLER TOLEDO, maximum =5.1 g; d =0.001 mg). To characterize the electrochemical behaviors, CHI440A (CH Instruments Inc. Shanghai) electrochemical workstation was used in a three-electrode electrochemical cell using a 6 M KOH aqueous solution as electrolyte. As to the asymmetric supercapacitor, two-electrode system was used. Electrochemical Impedance Spectroscopy (EIS) was tested on CS310 by applying an AC voltage with 5 mV amplitude in a frequency range from 0.01 Hz to 100 kHz at open circuit potential.

3 Results and discussion

3.1 Growth process and mechanism

CCNAs were successfully synthesized in a two-step hydrothermal method and CVD process. During the first hydrothermal step, the precursor was firstly synthesized according to the following formulas: [21]

$$Co^{2+} + 0.5(2-x)CO_3^{2-} + xOH^- + nH_2O \rightarrow Co(OH)_x(CO_3)_{0.5(2-x)} \cdot nH_2O \quad (1)$$

Then the precursor could be completely decomposed to CoO in the heating process as following equation:

$$Co(OH)_x(CO_3)_{0.5(2-x)} \cdot nH_2O \rightarrow$$

$$CoO + 0.5(2-x)CO_2 + (n+\frac{x}{2})H_2O \quad (2)$$

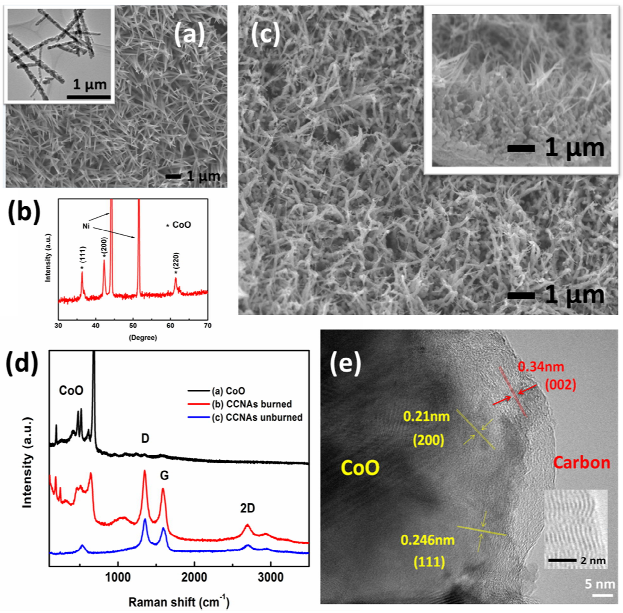

Fig. 2 (a,b) XRD spectrum, SEM, TEM images of CoO nanowires CCNAs-0s. (c) Top and side view of CCNAs-150s. (d) Raman spectrum of CoO nanowires, CCNAs-150s with partial carbon burned in a laser power 20 mW, CCNAs-150s in a laser power 0.2 mW. (e) HRTEM image of CCNAs-150s.

The XRD pattern of the annealed product CCNAs-0s (no C_2H_2 introduced) is shown in Fig. 2a, corresponding to the cubic structure CoO (JCPDS Card No. 48-1719) of (111), (200), (220) lattice plane. The ultrahigh peaks come from the substrate Ni. Patterns for CCNAs-0s, 120 s, 150s, 180s are displayed in Fig. S1a ESI. The peaks of CCNAs become weaker as the carbon were integrated. The morphology of the CCNAs-0s and CCNAs-150s are revealed by SEM and TEM, as depicted in Fig. 2b, c and e. The top view of the CCNAs-0s displays a vertical nanowires array in Fig. 2b. The inset TEM image shows the CoO nanowires are rough which are actually composed of single nanoparticles attached to each other resulting from the release of gases (CO_2, H_2O) in the calcination process. After the introduction of C_2H_2 for 150 s, the diameter of nanowires get thicker and the inset view reveals that the surface become a little smooth, indicating the surface of the wire is covered by something. The thickness of the whole electrode CCNAs is about 3~4 μm. Fig. 2d displays the Raman spectrum of CCNAs-0s, CCNAs-150s burned and CCNAs-150s to convince the existence of carbon after CVD stage. Curve (a) reveals the characteristic peaks at 185.0, 243.0, 459.0, 508.2, 597.1, 657.6 cm^{-1} of CoO.[22] Curve (c) is the spectrum of CCNAs-150s under the same test condition (laser power 0.2 mW) as that of CCNAs-0s. Obvious D, G, 2D peaks of carbon around 1356.0, 1593.8 and 2704.8 cm^{-1} imply that the carbon successfully deposits on the substrate with CoO.[23] The characteristic peaks of CoO in curve (c) are weaker compared to that in the curve (a) for the coverage of carbon on CoO. On this account, we enhanced the laser power to 20 mW to burn off portion of carbon and recorded its patterns in curve (b). It can be

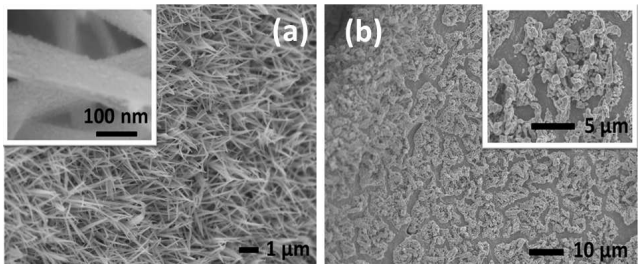

Fig. 3 SEM images of (a) CCNAs-120s and (b) CCNAs-240s.

clearly seen that all the characteristic peaks of CoO appear again, which is in good agreement with curve (a), confirming that the carbon successfully covers on the surface of CoO. The burned product (annealed in air at 800 ℃) was also further convinced as CoO through XRD results of CCNAs-150s and CCNAs-150s burned as shown in Fig. S1b ESI. In order to get more detailed information, we recorded high resolution TEM image of individual CCNAs-150s nanowire as shown in Fig. 2e. In the region of CoO, two interplanar spacings of 0.21 and 0.246 nm can be clearly observed, resulting from (200) and (111) lattice planes of CoO. At the edge of the wire, well crystalline covering layer was found. 0.34 nm interplanar distance matches well of graphite (002) plane, indicating the formation of crystalline graphite carbon.

In the experiments, the C_2H_2 ventilation time plays an important role in the morphology and electrochemical behaviors of CCNAs, a series of ventilation time-dependent experiments (0 s, 120 s, 150 s, 180 s and 240 s) were carried out. SEM images reveal great change of the sample morphology with the C_2H_2 ventilation time increase. Without introduction of C_2H_2 (0 s), the rough CoO nanowires were formed and grown uniformly and vertically on the Ni foam (Fig. 2b), which benefits the deposition of carbon. When the C_2H_2 ventilation time was 120 s, some carbon dots (~5 nm) coated on the surface of nanowires were observed in the inset high magnification SEM image in Fig. 3a. With the time of ventilation extending to 150 s, the nanowires were covered with layers of graphite instead of carbon dots (Fig. 2c) and no obvious morphological changes were found for additional 30 s of C_2H_2 ventilation (CCNAs-180s, image not shown). But when the time was increased to 240 s, the array structure was destroyed and loose bulk structure constructed of many particles dominated (Fig. 3b). The low magnification SEM images of CCNAs-0s, 120 s, 150 s, 240 s is shown in Fig. S1a ESI and the growth process is further discussed in ESI. Thus from the view of morphology, ventilation time between 150 s and 180 s is considered as the optimum duration for the synthesis of CCNAs. To confirm the strong coupling between CCNAs and the substrate, CCNAs-150s received a sonication test lasting for up to 1 h. No visible change can be observed from the magnified SEM and TEM images. This feature might be quite significant for enhancing the capacitive properties, which will be discussed shortly.

To clearly investigate the carbon deposition process and

growth mechanism, EDS elemental mappings of CCNAs-150s were performed to confirm the element distribution. Fig. 4a gives a TEM image of an individual wire covered with carbon, which confirms a CoO/C core-shell structure forms. Fig. 4b and Fig. 4c show a HADDF-STEM image and O, Co, C elemental distribution taken from the red and yellow circle part, respectively. The mappings show the carbon completely occupies the surface of CoO. Interestingly, the intensity of O signal is obviously weaker than that of Co in both (b) and (c), signifying that the content ratio of oxygen to cobalt is less than 1 (O/Co<1) in the surface of CCNAs-150s. For comparison, a HADDF-STEM image and O, Co, C elemental distribution of CCNAs-0s is shown in Fig. 4(d). It can be seen that only a little C covers the

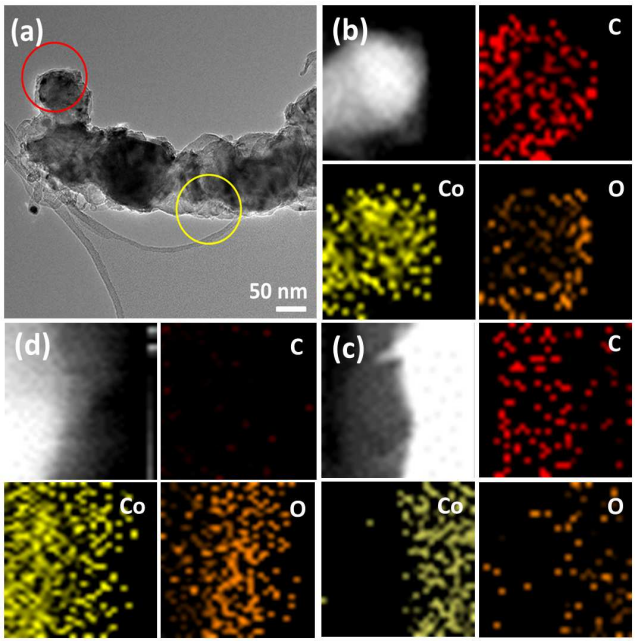

Fig. 4 (a) TEM images of individual CCNAs-150s. (b) Elemental mappings corresponding to the red circle in (a). (c) Elemental mappings corresponding to the yellow circle in (a). (d) Elemental mappings of CCNAs-0s.

nanowire and the content ratio of oxygen to cobalt (O/Co) is obviously larger than that in (b) and (c). This suggests that the ratio of O/Co in the surface of CoO has some effect on the carbon

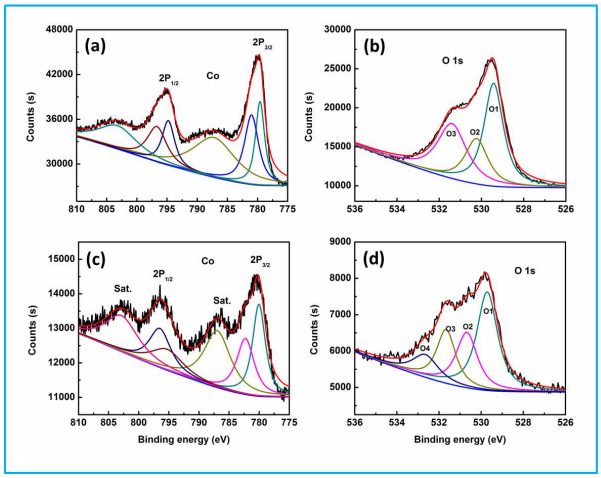

Fig. 5 High-resolution XPS spectrum of CCNAs-0s ((a) Co 2p, (b) O 1s) and CCNAs-150s ((c) Co 2p, (d) O 1s).

deposition during CVD stage. This will be discussed in detail in combination with the XPS data later.

The more detailed elemental composition and valance state of both CoO nanowires CCNAs-0s and CCNAs-150s are further characterized by XPS measurements and the results are presented in Fig. 5. Fig. 5a, c is the high-resolution XPS spectrum of Co 2p and O 1s for CoO, and Fig. 5b, d is of Co 2p and O 1s for CCNAs-150s, respectively. Carbon 1s spectrum (not given) is used for calibration (284.6 eV). By using a Gaussian fitting method, the Co 2p emission spectrum is best fitted with two spin orbit doublets, characteristic of Co^{2+} and Co^{3+} and two shakeup satellites. The obvious satellites in Fig. 5c suggest the Co 2p mainly comes from CoO, and the Fig. 5a agrees with the Co_3O_4,[24] indicating that the surface of CCNAs-0s has been oxidized to Co_3O_4 in air. It is because that the surface of CoO exposed in air (when the sample was taken out) is readily oxidized to Co_3O_4 to keep stable.[25] As to CCNAs-150s, carbon integrated on the surface of CoO protected the CoO from being oxidized, so the signals of CoO were mainly detected. Fig. 5b shows three oxygen contributions, the O1 529.4 eV is attributed to the typical metal oxygen bonds.[25] O2 and O3 peaks at 530.2 and 531.4 eV are associated with hydroxyl groups and absorbed water.[26-27] However, the O 1s peak of CCNAs-150s contains a well-resolved O4 at a higher 532.7 eV, which is few observed in cobalt oxides. In Sexton's work,[28] they reported that when the CoO was reduced to the atomic ratio of O/Co less than 1, an O 1s peak around 532.7 eV would appear. So we can conclude from Fig. 5d that the atomic ratio of O/Co is less than 1 in the CoO core surface of CCNAs-150s, which is in agreement with the results of EDS mappings analysis. Thus such ventilation process could be convinced as a mild surface reduction reaction.

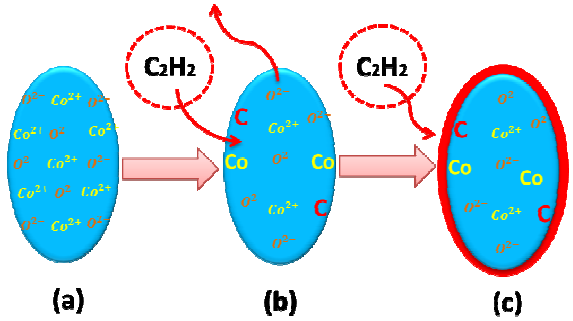

Fig. 6 Growth mechanism of CCNAs from CoO.

Considering above results: (i) The O/Co ratio is less than 1; (ii) The effect of C_2H_2 on the CoO is a mild surface reduction reaction. (iii) Only Co atoms but not Co^{2+} could catalyze the decomposition of C_2H_2 to crystalline carbon in this experiment, we proposed the growth mechanism of CCNAs from CoO as illustrated in Fig. 6. A fresh surface of CoO is obtained after 3 h annealing. As the reducing gas is introduced at 427 ℃, Co^{2+} on the surface tends to be reduced to Co, and some amorphous carbon dots begins to deposit on the reaction area as illustrated in

Fig. 6 (a)-(b). Meanwhile, O^{2-} bonding with the reduced Co^{2+} transfers to the surface and deviates in certain forms of $C_xH_yO_z$ or H_2O, which lead to a O/Co ratio less than 1. After that, partial Co in the surface of CoO catalyze the decomposition of C_2H_2 in a low temperature, forming carbon. The carbon dissolve in Co and segregate to form few layers graphene or graphite as shown in TEM image and illustrated in Fig. 6 (b)-(c).[29] The strategy may provide the possibility to fabricate one-dimensional graphene arrays for a number of potential applications.

3.2 Results, discussions and applications

In this work, CCNAs are designed as more conductive carbon on rough metal oxides nanowires which directly grow on the 3D nickel foam current collector. The electrochemical tests were carried out using a three-electrode reference electrode in 6 M KOH aqueous electrolyte. Electrodes being treated with different ventilation time, CCNAs-0s, CCNAs-120s, CCNAs-150s and CCNAs-180s were studied to investigate the optimal growth conditions. Each of the electrodes to be tested was cut into 2 × 0.5 cm^2 as working electrodes.

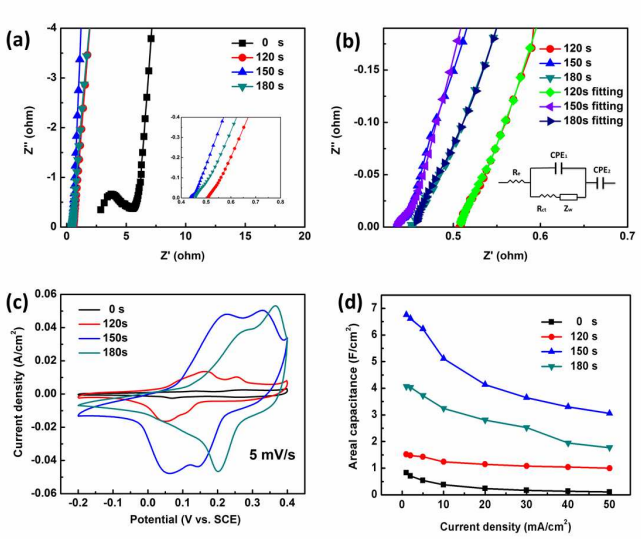

Fig. 7 (a) EIS spectrum, (c) CV curves in the potential window -0.2 V to 0.4 V and (d) Areal capacitance versus various current densities of all the four samples. (b) High frequency EIS curve fitting for the samples CCNAs-120s, 150s, 180s and equivalent circuit of the electrochemical system.

EIS is used to characterize the fundamental behavior of supercapacitor electrodes. The corresponding Nyquist plots of CCNAs-0s, 120s, 150s, 180s are shown in Fig. 7a which illustrate a combined resistance R_s (ionic resistance of electrode, intrinsic resistance of substrate, and contact resistance at the active material/current collector interface, the intersection of the curve at real part), a charge-transfer R_{ct} (the semicircle diameter), and Warburg resistance Z_w (ion diffusion/transport in the electrolyte to the electrode surface, slope of the curve at low frequency). According to the Nyquist plots shown in Fig. 7a, the CCNAs-0s possess a relatively vertical Z_w in the low frequency region, indicating that the rough CoO nanowire arrays are suitable for supercapacitor. However, its high intrinsic resistance restrains the electrochemical performance. Obviously, with the carbon incorporated, electrical conductivity of CCNAs-120s, CCNAs-150s and CCNAs-180s are dramatically promoted. The enhanced electrical behaviors are closely related to the property of deposited carbon, which can be revealed from the Raman spectrum in Fig. 2d. As reported,[30] the G band originates from the E_{2g} stretching mode of graphite, which is closely related to the vibration of sp^2 bonded carbon atoms in a 2D hexagonal lattice. The D band reflects the graphite-structure imperfection. The 2D band originates from a two phonon double resonance Raman process, so it is closely related to the band structure of graphene layers.[31] For CCNAs-150s, the obvious symmetric 2D peak and the ratio band G/2D is 3.77, which manifests the existence of few layers graphite close to graphene. The intensity ratio of D to G band is calculated to be ~ 1.4, which indicates the existence of disordered carbon and structural defects. The high ratio values of D/G and G/2D are because of the low temperature during the synthetic process compared to others (T≥900K).[32-34] However, the existence of structural defects make it easier to form hydrophilic oxygen functional groups[29] on the CCNAs-150s surface, which make the CCNAs-150s electrode much higher specific capacitance due to more efficient surface utilization in aqueous electrolyte.[35-36] Water contact angle measurement was taken to further verify the promotion of hydrophily as the carbon was introduced. The images of water contact angle of CCNAs-0s and CCNAs-150s on nickel foam are shown in Fig. S3 ESI. Meanwhile, well crystalline graphite carbon dramatically increases the electrical conductivity, which compensates for the intrinsic shortcomings of CoO. As a consequence, the promotion of the R_s at the same electrolyte is because of the hydrophilic oxygen functional groups on the surface introduced by carbon. Moreover, the absence of complete semicircle regions for CCNAs-120s, CCNAs-150s and CCNAs-180s indicate low faradaic resistance of the hybrid arrays and good electrical conductivity between arrays and the nickel foams,[38-39] which is mainly due to a more compacted structure on account of the deposition of carbon. To further research the property in the high frequency part, the electrochemical system is fitting in the equivalent circuit of Fig. 7b. Through curve fitting, resistances of the samples 0s (not shown), 120s, 150s, 180s are about R_e: 2.48 Ω, 0.51 Ω, 0.44 Ω, 0.46 Ω and R_{ct}: 2.85 Ω, 0.16 Ω, 0.03 Ω, 0.11 Ω, respectively. Overall, the resistances of the samples with carbon are much lower than that of CCNAs-0s. It's noteworthy that an impressive improvement of several orders of magnitude of the conductivity is received which is much higher than previous works, such as carbon modified MnO_2,[40] TiO_2,[41] CoO wrapped in PPy[8] and carbon nanomembrane.[9] Combined with above SEM, XRD, Raman results, we could further conclude that, with the increase of the ventilation time to 120 s, the disordered carbon forms on the surface of CoO. Consequently, more hydrophilic surface leads to a lower R_e in the aqueous solution. With the ventilation continuing to 150 s, the graphite covers the rods and a fast ion channel is constructed, thus the R_{ct} greatly reduces and similarly to the Z_w. When the time is more than 180 s, CCNAs structure start to collapse and electroactivity goes down.

Fig. 7c shows the Cyclic voltammograms (CV) curves of the samples CCNAs-0s, 120s, 150s and 180s at the scanning rate of 5 mV s^{-1} in the potential range of -0.2 to 0.4 V. For the all electrodes, two pairs of redox peaks in the alkaline electrolyte can

be observed. The pair of redox peaks in the low potential are derived from Co^{2+}/Co^{3+} interconversion (Equation 3), while pairs of peaks in the high potential are for conversion between Co^{3+} and Co^{4+} (Equation 4). The redox reactions in the alkaline electrolyte are described as following equations:

$$CoO + OH^- \leftrightarrow CoOOH + e^- \quad (3)$$

$$CoOOH + OH^- \leftrightarrow CoO_2 + H_2O + e^- \quad (4)$$

Pure nickel foam is also analyzed and could be negligible compared to CoO arrays CCNAs-0s. Fig. 7c reveals that the peaks shift right for two pairs of redox peaks with the carbon deposition time, mainly due to a higher over potential derived from the performance boost. For cobalt oxides, Co^{3+}/Co^{4+} interconversion usually dominates the redox action and receives a distinct higher peak value.[3, 8, 36] However, for samples CCNAs-120s and 150s, Co^{2+}/Co^{3+} peaks are higher or comparable to Co^{3+}/Co^{4+}. Such result illustrates that carbon introduced primarily facilitates Co^{2+}/Co^{3+} interconversion, meanwhile the Co^{3+}/Co^{4+} pattern is further improved for more Co^{3+} received.

The galvanostatic charge/discharge tests have been conducted at various current densities from 1 mA cm^{-2} to 50 mA cm^{-2} for all the samples. Fig. 7d shows the area capacitance behaviors of CCNAs with the average array thickness of about 4 μm. The highest area capacitance is 0.827, 1.516, 6.961 and 4.065 F cm^{-2} at a current density of 1 mA cm^{-2} for samples CCNAs-0s, 120s, 150s and 180s, respectively. Capacitance performance receives a significant improvement as to CCNAs-150s and begins to descend for the sample CCNAs-180s. The results are in agreement with the area of CV loop curves. Meanwhile, rate capability is also further raised from retention 12.7% (0 s) to at least 45.2 % (180 s) in the range of 1~50 mA cm^{-2}, which indicates the material better rate capability. Carbon incorporated plays an important role in promotion of the fast ion diffusion, intrinsic and reducing the contact resistance, as discussed in EIS spectrum.

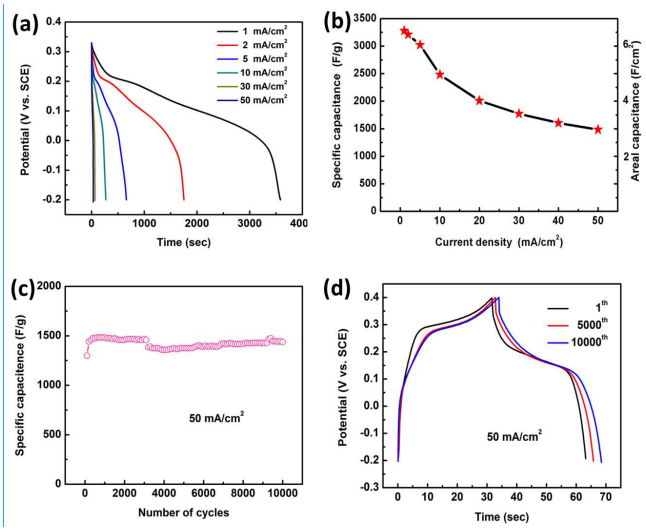

Fig. 8 Electrochemical performance of CCNAs-150s: (a) Discharge curves. (b) Capacitance behaviors versus current density. (c) Cycling performance at the current density of 50mA cm^{-2}. (d) Charge-discharge curves of the 1th, 5000th, 10000th cycle.

Based on above discussion, CCNAs-150s possesses the best electrical conductivity and electroactivity among the products. The galvanostatic charge/discharge tests have been conducted at various current densities from 1 mA cm^{-2} to 50 mA cm^{-2} in the potential window between -0.2 V and 0.33 V (Fig. 8a). At a current density of 1mA cm^{-2}, an ultrahigh discharge time 3583.5 s expresses its excellent electrochemical property, which is calculated as high as 3282.2 F g^{-1} and area capacitance 6.76 F cm^{-2}. Fig. 8b shows the capacitance behaviors versus various current densities. At higher current densities of 5, 10, 20 and 50 mA cm^{-2}, the hybrid electrode retains 3022.0, 2483.0, 2009.5 and 1483.8 F g^{-1} with a relatively high mass loading 2.06 mg cm^{-2}, which is the highest than those of many other nanostructures containing cobalt oxides or carbon materials to our best knowledge. Such as Co_3O_4 nanosheets (2735 F g^{-1} at 2 A g^{-1}),[42] Co_3O_4/carbon nanomembrane (1086 F g^{-1} at 1 mV s^{-1}), [11] CoO/$Ni(OH)_2$ (2374.0 F g^{-1} at 1.03 A g^{-1}),[3] CoO/PPy (2223 F g^{-1} at 1mA cm^{-2}).[8] The excellent cycling performance is illustrated in Fig. 8c by the long-term cycling test at a high current density of 50 mA cm^{-2}. 96.9% capacitance retention is found during the 10000 cycles and there even exists a rising trend. Such outstanding cycling performance is further evidenced by the chosen 1th, 5000th, 10000th charge-discharge curves in Fig. 8d. The discharge time extends as the times increase; furthermore, the CCNAs-150s maintains an excellent electrochemical reversibility with nearly 100% Coulombic efficiency all the time, suggesting the improvement of conductivity and the hybrid electrode a great potential application.

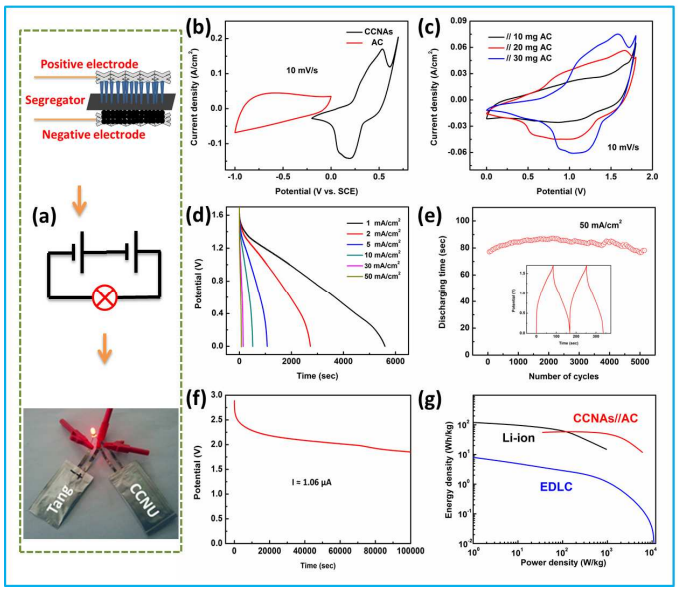

Fig. 9 (a) Configuration of the asymmetric supercapacitor. (b) CVs of the CCNAs-150s and AC from -1V to 0 V, -0.2 V to 0.7 V respectively. (c) CVs of the CCNAs//AC with different AC masses. (d) Discharge curves of CCNAs//AC versus various current density. (e) Cycling performance at the current density 50 mA/cm^2 and the symmetric charge-discharge curve. (f) Self-discharge curve of two asymmetric supercapacitor devices in series. (g) Ragone plot of CCNAs//AC device compared with Li-ion battery and EDLC.[8]

To test the practical application of the material, an aqueous 1 × 1 cm^2 asymmetric full cell of supercapacitor device (CCNAs//AC) was assembled through integrating CCNAs-150s as the positive

electrode and activated carbon (AC) as negative electrode film on pressed nickel foam in 6 M KOH electrolyte with one piece of cellulose paper as the separator in a two-electrode system as shown in Fig. 9a. The CV curves of the CCNAs-150s and AC from -1V to 0 V, -0.2 V to 0.7 V respectively at 10 mV s^{-1} curve in a three-electrode system, which implies the overall potential window could be as large as 1.7 V (see Fig. 9b). Different AC masses loaded also determine the capacitance behaviors. Using AC mass of 10 mg, 20 mg, 30 mg as negative electrodes, respectively, and CCNAs-150s as positive electrode are fabricated as full cells. When the loading mass of AC is more than 10 mg, apparent redox peaks reveal, suggesting the electrochemical behaviors of CCNAs dominates. As the mass increases to 30 mg, more obvious peaks are found but the oxidation current rises dramatically, which implies the evolution of gas and an unstable device (Fig. 9c). When employed 20 mg AC film as negative electrode, the device possesses a high energy of 58.9 Wh kg^{-1} at a power density 198.7 W kg^{-1} (Fig. 9d, g), which is comparable with the Li-battery and highest among the Co-based supercapacitor devices, such as reduced graphene oxide/Co_3O_4//AC, 47.2 Wh kg^{-1} at 200.6 W kg^{-1},[43] 35.7 Wh kg^{-1} at 225 W kg^{-1} ,[44] and CoO@PPy//AC 43.5 Wh kg^{-1} at 81.5 W kg^{-1}.[8] When the power density increases to 3186.5 W kg^{-1} (100 mA), the energy still remains 25.84 Wh kg^{-1}. The discharge curves versus various current densities and cycling performance are also given in Fig. 9d, e. Excellent cycling performance and Columbic efficiency are also received just as in the three-electrode device. In addition, we assembled two devices in series to form a device with potential more than 3 V to test the practical application. After charging the 3 V device for 15 s, it could power a red 5 mm LED light (2.5 V, 20 mA) as shown in Fig. 9a. Meanwhile, we also performed the self-discharge test to manifest the energy-storage behaviors. Fig. 9f displays the self-discharge curve of the device after precharging to 3 V. In the whole self-discharging test, the discharging current remained as low as 1.06 μA. After discharge for 100000 s, the potential still remained as high as 1.85 V, signifying good encapsulation and promising practical applications.

4 Conclusions

In summary, a low temperature in-situ CVD method to fabricate CCNAs based on 3D nickel foam is developed to boost the electrochemical behaviors of CoO. In an optimized condition, the CCNAs receive an ultrahigh specific capacitance of 3282.2 F g^{-1} approaching to the theoretical value on accounts of low resistance and a more hydrophilic surface introduced by deposited crystalline and strongly coupled carbon. Good rate capability and 96.9% capacitance retention after 10000 cycles suggest such hybrid electrode possesses a great potential application. The growth mechanism is proposed by TEM, XPS analysis. After assembling it as positive electrode and activated carbon as the negative electrode, the aqueous asymmetric supercapacitor demonstrates energy density up to (~58.9 Wh kg^{-1} at 198.7 W kg^{-1}), which is the highest energy density received among the Co-based supercapacitors. Our work demonstrates a new strategy to fabricate graphite carbon/cobalt monoxide nanostructure arrays, which provides not only a feasible method for arbitrary cobalt oxides to combine with high-quality carbon but also a possibility to fabricate one-dimension graphene arrays.

Acknowledgment

Financial supported by the key program of the Natural Science Foundation of Hubei Province (2012FFA080).

Notes and references

Institute of Nanoscience and Nanotechnology, Department of Physics, Central China Normal University, Wuhan, 430079, China. Fax:86 27 67867947;Tel.: :86 27 67867947; E-mail: ywtang@phy.ccnu.edu.cn

1 (a) J. R. Miller, P. Simon, *Science* 2008, 321, 651; (b) P. Simon and Y. Gogotsi, *Nat. Mater.*, 2008, **7**, 845.
2 H. Jiang, J. Ma and C. Z. Li, *Adv. Mater.*, 2012, **24**, 4197.
3 C. Guan, X. L. Li, Z. L. Wang, X. H. Cao, Cesare Soci, H. Zhang and H. J. Fan, *Adv. Mater.*, 2012, **24**, 4186.
4 X. H. Xia, J. P. Tu, Y. J. Mai, X. L. Wang, C. D. Gu and X. B. Zhao, *J. Mater. Chem.*, 2011, **21**, 9319.
5 J. H. Zhu, J. Jiang, J. P. Liu, R. M. Ding, Y. M. Feng, G. M. Wei, X. T. Huang, *J. Solid State Chem.*, 2011, **184**, 578.
6 C. C. Hu, K. H. Chang, M. C. Lin, Y. T. Wu, *Nano Lett.*, 2006, **6(12)**, 2904.
7 (a) S. Chen, J. W. Zhu, X. D. Wu, Q. F. Han, X. Wang, *ACS Nano,* **4(5)**, 2822. (b) X. Y. Lang, A. Hirata, T. Fujita and M. W. Chen, *Nat. Nanotechnol.*, 2011, **6**, 232.
8 C. Zhou, Y. W. Zhang, Y. Y. Li and J. P.Liu, *Nano Lett.*, 2013, **13**, 2078.
9 C. C. Xiang, M. Li, M. J. Zhi, A. Manivannan, N. Q. Wu, *J. Power Sources*, 2013, **226**, 65.
10 Y. Y. Liang, H. L. Wang, P. Diao, Wesley C, G. S. Hong, Y. G. Li, M. G, L. M. Xie, J. G. Zhou, J. Wang, Tom Z. Regier, Fei Wei and H. J. Dai, *J. Am. Chem. Soc.*, 2012, **134**, 15849.
11 J. Zhi, S. Deng, Y. X. Zhang, Y. F. Wang, A. G. Hu, *J. Mater. Chem. A,* 2013, **1**, 3171.
12 Z. C. Yang, C. H. Tang, Y. Zhang, H. Gong, X. Li and Jorn Wang, *Scientific Reports*, 2013, **3**, 2295
13 (a) M. Volder, S. H. Tawfick, R. H. Baughman, A. J. Hart, *Science*, 2013, **339**, 535; (b) R. F. Zhou, C. Z. Meng, F. Zhu, Q. Q. Li, C. H. Liu, S. S. Fan and K. L. Jiang. *Nanotechnol.*, 2009, **20**, 204023.
14 X. W. Yang, C. Cheng, Y. F. Wang, L. Qiu, D. Li, *Science*, 2013, **341**, 534.
15 J. Gamby, P. L. Taberna, P. Simon, J. F. Fauvarque, M. Chesneau. *J. Power Sources*, 2001, **101**, 109.
16 L. M. Dai, D. Wook Chang, Jong-Beom Baek and W. Lu, *Small*, 2012, **8**, 1130.
17 M. J. Zhi, C. C. Xiang, J. T. Li, M. Li and N. Q. Wu , *Nanoscale*, 2013,**5**,72.
18 S. L. Xiong, J. S. Chen, X. W. Lou and H. C. Zeng, *Adv. Funct. Mater.*, 2012, **22**, 861.
19 T. Xiao, B. J. Heng, X. Y. Hu, Y. W. Tang, *J. Phys. Chem. C*, 2011, **115**, 25155.
20 (a) Y. Huang, Y. Y. Li, Z. Q. Hu, G. M. Wei, J. L. Guo and J. P. Liu, *J. Mater. Chem. A*, 2013, **1**, 9809; (b) J. Chen, X. H. Xia, J. P. Tu, Q. Q. Xiong, Y. X. Yu, X. L. Wang and C. D. Gu, *J. Mater. Chem.,* 2012, **22**, 15056.
21 J. Jiang, J. P. Liu, R. M. Ding, X. X. Ji, Y. Y. Hu. X. Li, A. Z. Hu, F. Wu, Z. H. Zhu and X. T. Huang, *J. Phys. Chem. C*, 2010, **114**, 929.
22 C. W. Tang, C. B. Wang, S. H. Chien, *Thermochim. Acta*, 2008, **473**, 68.
23 A.N. Obraztsov, A.V. Tyurnina, E.A. Obraztsova, A.A. Zolotukhin, B. Liu, K.C. Chin, A.T.S. Wee, *Carbon*, 2008, **46**, 963.
24 M. C. Biesinger, B. P. Payne, A. P. Grosvenor, L. Lau, A. R. Gerson, R. Smart, *Appl. Surf. Sci.*, 2011, **257**, 2717.

25 B. J. Tan, K. J. Klabunde and P. M. Sherwood, *J. Am. Chem. Soc.,* 1991, **113**, 855.
26 N. S. Mclntrye, M. G. Cook, *Anal. Chem*. 1975, **47**, 1975.
27 T. J. Chuang, C. R. Brundle, D. W. Rice, *Surf. Sci.* 1976, **59**, 413.
28 B. A. Sexton, A. E. Hughes and T. W. Turney, *J. Catal.* 1986, **97**, 390.
29 M. E. Ranmon, A. Gupta, C. Corbet, D. A. Ferrer, H. C. Movva, G. Carpenter, L. Colombo, G. Bourianoff, M. Doczy, D. Akinwande, E. Yuyuc and S. K. Banerjee, *ACS Nano*, 2011,**5(9)**, 7198.
30 Z. H. Ni, H. M. Fan, Y. P. Feng, Z. X. Shen, B. J. Yang, *J. Chem. Phys*. 2006, **124**, 204703.
31 Z. H. Ni, Y. Y. Wang, T. Yu and Z. X. Shen, *Nano Res.*, 2008, **1**, 273.
32 D. Mattia, M. P. Rossi, B. M. Kim, G. Korneva, H. H. Bau and Y. Gogotsi, *J. Phys. Chem. B*, 2006, **110**, 9850.
33 Y. Q. Wu, Y. M. Lin, A. A. Bol, K. A. Jenkins, F. N. Xia, D. B. Farmer, Y. Zhu and P. Avouris, *Nature* 2011, **472**, 74.
34 Q. K. Yu, J. Lian, S. Siriponglert, H. Li, Y. P. Chen and S. S. Pei, *Appl. Phys. Lett*., 2008, **93**, 113103.
35 H. Zhang, G. P. Cao and Y. S. Yang, *Energy Environ. Sci.*, 2009, **2**, 932.
36 D. Y. Qu, *J. Power Sources* 2002, **109**, 403.
37 A. G. Pandolfo, A. F. Hollenkamp, *J. Power Sources* 2006, **157**, 11.
38 Q. Wu, Y. X. Xu, Z. Y. Yao, A. Liu and G. Q. Shi, *ACS Nano*, 2010, **4(4)**, 1963.
39 G. X. Pan, X. Xia, F. Cao, P. S. Tang, H. F. Chen, *Electrochimica Acta*, 2012, **63**, 335.
40 Y. Huang, Y. Y. Li, Z. Q. Hu, G. M. Wei, J. L. Guo and J. P. Liu, *J. Mater. Chem. A,* 2013, **1**, 9809.
41 J. Y. Liao, D. Higgins, G. Lui, V. Chabot, X. C. Xiao, Z. W. Chen, *Nano Lett*. 2013, **13(11)**, 5467.
42 L. Cao, F. Xu, Y. Y. Liang, H. L. Li, *Adv. Mater.*, 2004, **16**, 1853.
43 C. Z. Yuan, L. Yang, L. R. Hou, L. F. Shen, X. G. Zhang and X. W. Lou, *Energy Environ. Sci.*, 2012, **5**, 7883.
44 C. C. Xiang, M. Li, M. J. Zhi, A. Manivannan, N. Q. Wu, *J. Power Sources*, 2013, **226**, 65.
45 L. J. Xie, J. F. Wu, C. M. Chen, C. M. Zhang, L. Wan, J. L. Wang, Q. Q. Kong, C. X. Lv, K. X. Li and G. H. Sun, *J. Power Sources*, 2013, **242**, 148.

Graphical Abstract

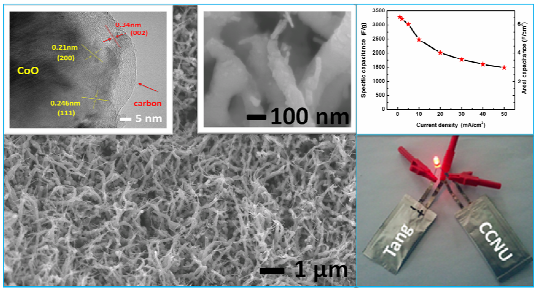

Highly conductive carbon grown on rough CoO nanowire arrays electrodes on 3D nickel foam were designed with an ultrahigh specific capacitance of 3282.2 F g^{-1} approaching to the theoretical value of CoO. When assembled into an asymmetric supercapacitor device, an energy density (~58.9 Wh kg^{-1}) is obtained which is the highest among the Co-based supercapacitors.